Contents lists available at ScienceDirect

Aquaculture

Internal carbohydrates and lipids as reserved energy supply in the pubertal molt of *Scylla paramamosain*

Wenfeng Li [a,b], Shuang Li [a,b], Xiaofei Wang [a,b], Hui-yun Chen [a,b], Hua Hao [a,b], Ke-Jian Wang [a,b,c,*]

[a] *State Key Laboratory of Marine Environmental Science, College of Ocean & Earth Sciences, Xiamen University, Xiamen, Fujian, China*
[b] *State-Province Joint Engineering Laboratory of Marine Bioproducts and Technology, Xiamen University, Xiamen, Fujian, China*
[c] *Fujian Innovation Research Institute for Marine Biological Antimicrobial Peptide Industrial Technology, College of Ocean & Earth Sciences, Xiamen, Fujian, China*

ABSTRACT

Pubertal molt is critical for the reproductive process of mud crab *Scylla paramamosain*, during which female crabs molt and mate with males, and subsequently, ovarian development is initiated. Since fasting occurs during pubertal molt, the mechanism underlying how the internal energy reserves support crabs' survival is unclear. In this study, the hepatopancreas and ovaries were collected for metabolomics analyses. The results show 11 carbohydrate and 4 lipid metabolic pathways were remarkably modulated in hepatopancreas, suggesting carbohydrates and lipids may be the main energy reserves in hepatopancreas postmolt. Further analysis showed that the levels of glucose, glucose 6-phosphate, glucose 1-phosphate, and fructose 6-phosphate were increased, indicating glycolysis was upregulated for energy supply. Meanwhile, 65 lipids were significantly changed, including 16 glycerophospholipids and 33 fatty acids, suggesting lipids might be another main energy supplier in the hepatopancreas. In the ovary, 7 carbohydrate and 1 lipid metabolic pathways were obviously affected, and 12 carbohydrates and 23 lipids were also significantly changed postmolt. Differently from the changes in the hepatopancreas, the glucose level was significantly decreased in the ovary, whereas the levels of eight glycerophospholipids and four unsaturated fatty acids were increased in the ovary but decreased in the hepatopancreas, suggesting lipids might be major energy reserves for ovarian development, and they were possibly exported from hepatopancreas. Moreover, the obvious changes in seven fatty acyl carnitines in the ovary indicate they were consumed via β-oxidation postmolt. Taken together, carbohydrates and fatty acyl carnitines were clearly the major energy reserves in pubertal molt. The hepatopancreas played a central role in the supply of energy reserves and nutrients. Numerous glycerophospholipids and unsaturated fatty acids may have accumulated in the ovary for the biosynthesis of egg yolk during ovarian development. This study suggests that proper increases in carbohydrate and lipid levels in crab feed ahead of pubertal molt may alleviate the effects of fasting and enhance successful reproduction.

1. Introduction

Scylla paramamosain, well-known as the mud crab, is one of the most commercially important crustaceans distributed along the coast of southern China and the broader Indo-Pacific countries (Shi et al., 2018). The production of cultured mud crab has reached levels of 157,712 tons in China (China Fishery Statistical Yearbook, 2019). Female mud crabs with mature ovaries usually fetch premium prices because their ovaries are considered a delicacy (Gong et al., 2015). The culturing of female mud crabs usually provides a higher return from the economic perspective (Khatun et al., 2009; Wang et al., 2015). Moreover, healthy female mud crabs with mature ovaries are essential for the cultivation of crab seeds in the mud crab aquaculture industry (Muhd-Farouk et al., 2016). As such, the investigation into the reproductive development of female mud crab is likely to provide new perspectives regarding the manipulation of ovarian maturation in the aquaculture industry.

Crustaceans are characterized by a rigid exoskeleton, which must be molted periodically for growth and development (Oliphant et al., 2018). Before pubertal molt, the mud crab grows quickly via frequent molting (every 5–30 days, personal observations). In pubertal molt, mating happens quickly after the end of molt, when the female is in the soft-shell condition, and ovarian development is initiated immediately (Fazhan et al., 2017). Pubertal molt is essential for the reproductive development of female mud crabs. A comprehensive understanding of pubertal molt is beneficial for the cultivation of mature female mud crabs.

Crustaceans naturally fast during molt. Feeding stops completely during molting and begins again postmolt when the animal has an exoskeleton rigid enough to support its body weight and handle food (Chan et al., 1988; Rivera-Pérez and García-Carreño, 2011). No food intake (fasting) can lead to a severe deficiency in nutrients during molting, as only internally reserved nutrients are available (Sánchez-Paz et al., 2006). Researchers found a high incidence of molt death syndrome, which refers to death in a partially molted condition or soon after molt. For mud crabs, molt death syndrome leads to high mortality rates, especially when the larvae molt from zoea VI to megalopa, and from megalopa to juvenile crabs (Williams et al., 1999; Holme et al., 2007). Although the cause of this problem is not fully understood, it is believed to be associated with inappropriate nutrition (Bowser and Rosemark, 1981; Holme et al., 2007). Few studies have been devoted to the influence of nutrition on the molting of crustaceans (Chang and Mykles, 2011). Molting requires a significant amount of energy (Niu et al., 2012). Nguyen et al. (2014) reported that cumulative molts were clearly affected by voluntary feed or energy intake levels, suggesting molt was triggered when the threshold of energy became sufficient. Taken together, this indicates that sufficient energy supply could be critical for successful molting, including pubertal molting.

However, the reports about preferential energy supply during molting (fasting) in crustaceans are severely contrasting (Sánchez-Paz et al., 2006). Protein was proposed as the primary source of energy at the beginning. Then, a series of studies on *Penaeus japonicus*, *Penaeus duorarum*, and *Crangon crangon* indicated that glycogen stores were rapidly depleted, lipids diminished progressively, and proteins were mobilized but more slowly (Sánchez-Paz et al., 2006). Moreover, the metabolic requirements of crustaceans during fasting appear to be species-specific. Protein was reported to be the first energy supply in *Hemigrapsus nudus* and *Penaeus esculentus* (Neiland and Scheer, 1953; Barclay et al., 1983). Carbohydrates were identified as the preferential energy supply in *Calanus finmarchicus* and *Palaemonetes argentinus* (Helland et al., 2003; Neves et al., 2004). Besides this, the energy metabolism during fasting may vary depending on the development stage. In the phyllosoma larvae of *Jasus edwardsii* starved for 6–11 days, lipids were the main energy source in the late stages of development, while protein catabolism seems to be more important in stage I (Ritar et al., 2003). Johnston et al. (2004) reported that the protease and lipase activities in phyllosoma larvae were significantly increased and decreased in stage I and IV, respectively, suggesting protein catabolism provided energy during food deprivation. In general, the differences in energy source usage during fasting showed high variability, and it is too unclear to suggest a standard metabolic profile (Sánchez-Paz et al., 2007). To eliminate the major energy reserves consumed during pubertal molting (fasting), it is necessary to establish the metabolic profiles of mud crab *S. paramamosain*.

Moreover, pubertal molting is generally believed to be the start of ovarian development in some crab species; subsequently, females begin to develop their ovaries rapidly (He et al., 2014; Jiang et al., 2020). During pubertal molting, male mud crabs mate with the females through spermatophore transfer, and this triggers the ovarian maturation process (Muhd-Farouk et al., 2016). Ovarian development demands high energy allocation, requiring an unusual balance in the resources partitioned between growth and reproduction (Capparelli and Flores, 2011). However, little is known about the mechanism underlying how the internal nutrients support survival and the initiation of ovarian development in the pubertal molt stage of *S. paramamosain*. As the principal organ of nutrient metabolism in crustaceans, the hepatopancreas plays vital roles in energy storage and breakdown, nutrient accumulation, and carbohydrate and lipid metabolism (Wang et al., 2014; Zhan et al., 2020). Glucose from dietary carbohydrate is first absorbed by the hepatopancreas epithelial cells and then transported throughout the organism, which is the same mechanism as that seen in the transport of fatty acids and amino acids (Wang et al., 2016). The ovary is the most important organ in the reproduction of female crabs (Zhou et al., 2019), and ovarian development relies on exogenous vitellogenesis and lipids (Yao et al., 2008). Metabolomics, which focuses on small molecular metabolites (<1000 Da), has been used to reveal the physiological and metabolic changes related to nutrition and diet, disease, and environmental toxicology in many aquaculture species (Alfaro and Young, 2018; Gao et al., 2018). In the present study, the hepatopancreas and ovaries were collected for metabolomics analyses. A comprehensive investigation was performed to elucidate the vital metabolic changes in hepatopancreas and ovary during pubertal molting. This work may provide the basis for a better understanding of the energy reserve requirements during pubertal molting.

2. Materials and methods

2.1. Experimental animals and sampling

Mud crabs (*S. paramamosain,* female, 120 ± 10 g, Supplementary Fig. 1A; Supplementary Fig. 2F-J male, 150 ± 10 g) were collected from a local mud crab farm in Zhangzhou city, Fujian province, China (23.93° N, 117.58° E). Each couple of crabs was reared in a water tank (80 cm × 60 cm × 40 cm) with filtered and aerated seawater at 27 °C, and fed with clams twice per day. All tanks with crab couples were checked for pubertal molt 4 times a day, and a real-time video surveillance system was used to track the whole process of pubertal molting and copulation. According to the descriptions of molting stages in previous studies (Phlippen et al., 2000; Corteel et al., 2009; Liu et al., 2021), the molting cycle of the mud crab was divided into three major stages based on morphological changes in the swim paddle (personal observation, Supplementary Fig. 2), namely, the post-molt (Supplementary Fig. 2A, B), inter-molt (Supplementary Fig. 2C, D, and E), and pre-molt (early pre-molt, Supplementary Fig. 2F and G; and late pre-molt, Supplementary Fig. 2H, I, and J) stages. Once the pubertal molting and copulation finished, the female crabs (250 ± 20 g, Supplementary Fig. 1B; Supplementary Fig. 2A) were captured for sampling. Female crabs before pubertal molting were determined by morphological changes in the swim paddle (Supplementary Fig. 2J) and were sampled as a control (Supplementary Fig. 1A). In total, 12 crabs in the pre- and post-pubertal molt groups were collected for sampling, respectively. The hepatopancreas (Supplementary Fig. 1C, D, arrow head) and ovary (Supplementary Fig. 1C, D, short arrow) of each crab was dissected. Each sample (50 mg) was packed separately using a slice of sterile aluminum foil, immediately frozen in liquid nitrogen, and stored at −80 °C until needed. The 12 hepatopancreas and ovary samples were randomly divided into 6 parallel samples for metabolomics profiling, respectively. The animal experiments were fully reviewed and approved by the Laboratory Animal Management and Ethics Committee of Xiamen University.

2.2. Metabolite extraction

Six hepatopancreas and ovary parallel samples from pre- and post-pubertal molt groups were used for metabolite extraction, respectively. In total, 50 mg of each sample was extracted with 1000 μL pre-cold extraction solution (acetonitrile/methanol/water = 2/2/1, with 1 μg/mL of internal standard, 2-chloro-*L*-phenylalanine). The metabolite extract from each sample was incubated at −20 °C for 60 min and
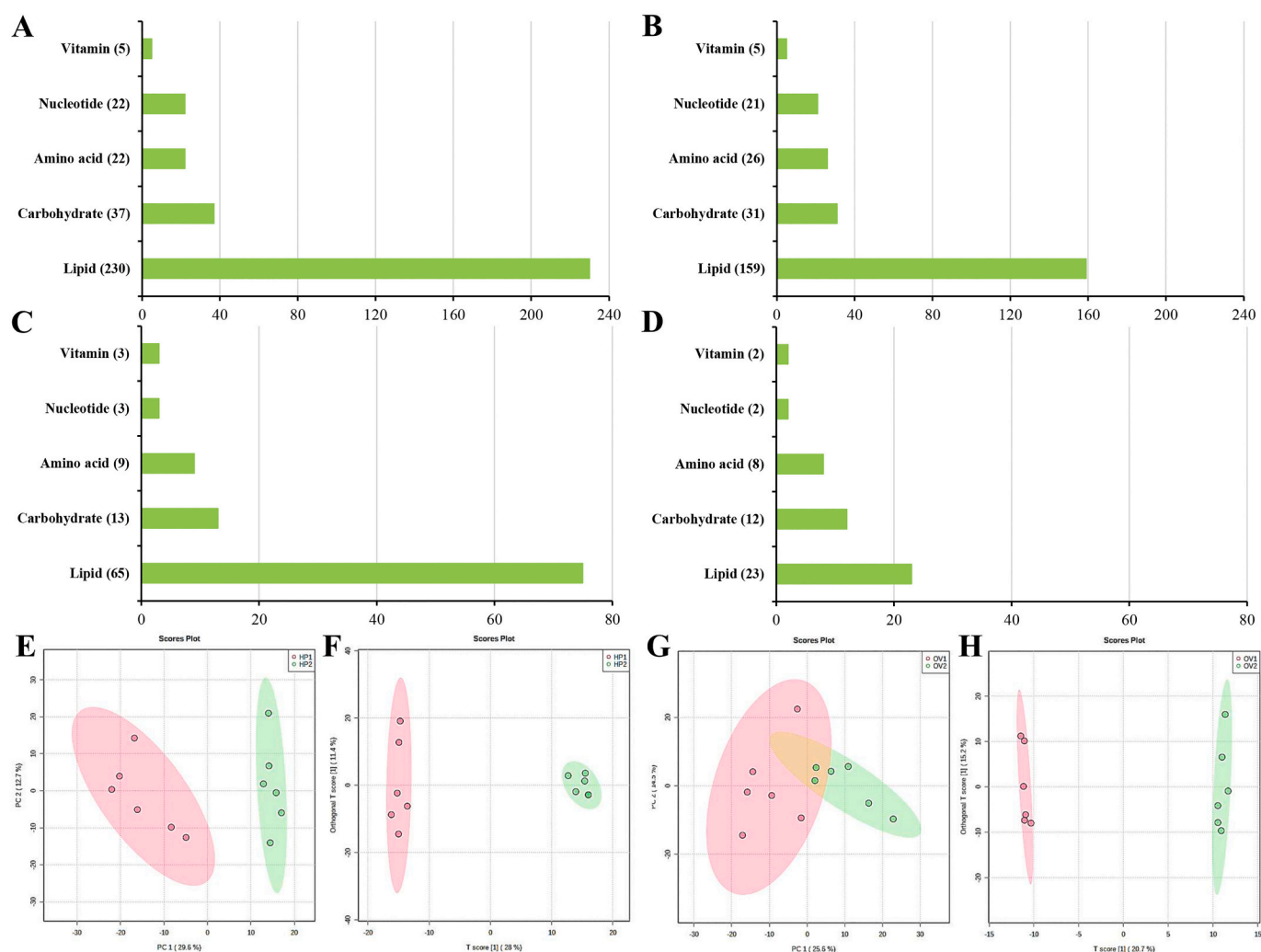
Fig. 1. Major metabolite classification (A, B) for the whole metabolomic profiles and for the significantly changed metabolites (C, D) of hepatopancreas and ovary, respectively. PCA score plot (E, F) and oPLS-DA score plot (G, H) for the metabolomic profiles of the hepatopancreas and ovary in the pre- and post-pubertal molting groups of *S. paramamosain*.

centrifuged at 12000 rpm at 4 °C for 15 min. The supernatant of each sample was collected and stored at −80 °C until LC-MS analysis. For the GC/TOF-MS analysis, a supernatant of each sample was evaporated in a vacuum concentrator and then incubated with 40 μL of methoxyamination hydrochloride (20 mg/mL in pyridine, TCI, Shanghai, China) for 30 min at 80 °C. Subsequently, 60 μL of N, O-bis (trimethylsilyl) trifluoroacetamide regent (1% trimethylchlorosilane, *v*/v, REGIS, Morton Grove, USA) was added to the sample aliquots, incubated for 90 min at 70 °C, and gradually cooled to room temperature. Before GC–MS analysis, 5 μL of saturated fatty acid methyl ester (in chloroform, Dr. Ehrenstorfer, Augsburg, Germany) was added into the QC sample. The quality control (QC) sample was prepared by mixing an equal aliquot of the supernatants from all samples to monitor the performance of data acquisition.

2.3. Liquid chromatography–mass spectrometry/mass spectrometry (LC-MS/MS)

LC-MS/MS detection was performed on a UHPLC system (1290, Agilent) with a UPLC HSS T3 column (2.1 mm × 100 mm, 1.8 μm, Waters) coupled with a Q Exactive mass spectrometer (Orbitrap MS, Thermo). The mobile phase A: 0.1% formic acid in water (positive) and 5 mmol/L ammonium acetate in water (negative), and B: acetonitrile. The elution gradient was set as follows: 0 min, 1% B; 1 min, 1% B; 8 min,

99% B; 10 min, 99% B; 10.1 min, 1% B; 12 min, 1% B. The flow rate was 0.5 mL/min and the injection volume was 3 μL. MS/MS spectra were acquired by mass spectrometer on an information-dependent basis (IDA). The acquisition software (Xcalibur 4.0.27, Thermo) continuously evaluated full-scan survey MS data depending on the preselected criteria. The ESI (electrospray ionization) source conditions were set as follows: the sheath gas flow rate, aux gas flow rate, capillary temperature, full MS resolution, and MS/MS resolution were 45 Arb, 15 Arb, 400 °C, 70000, and 17,500, respectively. The collision energy was 20/ 40/60 eV in the NCE model and the spray voltages were 4.0 kV (positive) and −3.6 kV (negative).

2.4. Gas chromatograph/time-of-flight mass spectrometer (GC/TOF-MS)

GC/TOF-MS analysis was performed using an Agilent 7890 gas chromatograph system with a DB-5MS capillary column (Agilent, Santa Clara, CA, USA), coupled with a time-of-flight mass spectrometer (Pegasus HT, Leco Corp., St. Joseph, MO, USA). Then, a 1 μL aliquot of each sample was injected in split-less mode. Helium was used as the carrier gas with a 3 mL/min front inlet purge flow and 1 mL/min gas flow through the column. The initial temperature was set at 50 °C for 1 min and was raised to 310 °C at a rate of 10 °C/min. The injection, transfer line, and ion source temperatures were set as 280 °C, 280 °C and 250 °C, respectively. The energy was set as −70 eV in the electron

Table 1
MetPA of the significantly changed metabolites in the hepatopancreas of *S. paramamosain* post-pubertal molt.

KEGG pathway subclass	KEGG Pathway	Total Compound	Hits	*p* value
Carbohydrate metabolism	Ascorbate and aldarate metabolism	6	2	1.09E-05
	Amino sugar and nucleotide sugar metabolism	34	3	0.00004
	Galactose metabolism	27	6	0.00006
	Pentose and glucuronate interconversions	16	2	0.00045
	Starch and sucrose metabolism	14	4	0.00055
	Inositol phosphate metabolism	28	2	0.00062
	Butanoate metabolism	14	1	0.00159
	Propanoate metabolism	21	2	0.00523
	Glycolysis / Gluconeogenesis	26	1	0.01017
	Citrate cycle (TCA cycle)	20	1	0.03313
	Glyoxylate and dicarboxylate metabolism	24	1	0.03313
Lipid metabolism	Sphingolipid metabolism	18	1	0.00012
	Alpha-Linolenic acid metabolism	8	1	0.00028
	Arachidonic acid metabolism	13	3	0.00090
	Glycerophospholipid metabolism	32	3	0.00142
Amino acid metabolism	Arginine biosynthesis	12	5	1.06E-06
	Arginine and proline metabolism	31	3	9.67E-06
	Histidine metabolism	9	2	0.00405
	Lysine degradation	21	1	0.00425
	Alanine, aspartate and glutamate metabolism	23	2	0.00501
Metabolism of other amino acids	Glutathione metabolism	26	4	4.80E-08
	Beta-alanine metabolism	14	4	0.00069
Metabolism of cofactors and vitamins	Pantothenate and CoA biosynthesis	18	5	0.00154
	Nicotinate and nicotinamide metabolism	9	1	0.00266
Nucleotide metabolism	Pyrimidine metabolism	40	4	2.27E-05
Translation	Aminoacyl-tRNA biosynthesis	48	8	0.00828
Signal transduction	Phosphatidylinositol signaling system	28	1	0.00265

Table 2
MetPA of the significantly changed metabolites in the ovary of *S. paramamosain* post-pubertal molt.

KEGG pathway subclass	KEGG Pathway	Total Compound	Hits	*p* value
Carbohydrate metabolism	Glycolysis/gluconeogenesis	26	2	0.00052
	Starch and sucrose metabolism	14	2	0.00135
	Pentose and glucuronate interconversions	16	2	0.00170
	Pentose phosphate pathway	22	1	0.00369
	Amino sugar and nucleotide sugar metabolism	34	1	0.00478
	Pyruvate metabolism	22	1	0.00781
	Glyoxylate and dicarboxylate metabolism	24	2	0.02795
Lipid metabolism	Sphingolipid metabolism	18	4	0.03288
Amino acid metabolism	Arginine biosynthesis	12	4	0.00000
	Glycine, serine and threonine metabolism	30	3	0.00024
	Tyrosine metabolism	33	1	0.00197
	Cysteine and methionine metabolism	32	2	0.00231
	Histidine metabolism	9	1	0.00589
	Tryptophan metabolism	30	2	0.01888
	Valine, leucine and isoleucine biosynthesis	8	2	0.01889
	Arginine and proline metabolism	31	1	0.02745
	Alanine, aspartate and glutamate metabolism	23	1	0.03568
Metabolism of other amino acids	Beta-alanine metabolism	14	2	0.00047
	Glutathione metabolism	26	3	0.00089
	D-glutamine and D-glutamate metabolism	5	1	0.03568
Metabolism of cofactors and vitamins	Pantothenate and CoA biosynthesis	18	4	0.00913
	Riboflavin metabolism	3	1	0.00933
Nucleotide metabolism	Purine metabolism	63	2	0.00960
	Pyrimidine metabolism	40	2	0.00684
Translation	Aminoacyl-tRNA biosynthesis	48	7	0.00196

impact mode. MS data were acquired in full-scan mode, and the *m/z* range was 50–500 at a rate of 12.5 spectra per second after a solvent delay of 6.25 min.

2.5. Metabolomic data preprocessing and identification

LC-MS/MS raw data were converted to the mzXML format using ProteoWizard (http://proteowizard.sourceforge.net/downloads.shtml), and were processed by MAPS software (version 1.0). The preprocessing results generated a data matrix, with retention time (RT), mass-to-charge ratio (m/z) and peak intensity values. Metabolite identification was performed with an in-house MS2 database (Biotree Biomedical Technology Co., Ltd., Shanghai, China). The GC-TOF-MS raw data were analyzed with the Chroma TOF (version 4.3×, LECO) software, including peak extraction, baseline adjustment, deconvolution, alignment, and integration. Metabolite identification was performed with the LECO-Fiehn Rtx5 database by matching the mass spectrum and the retention index. Peaks detected in fewer than half of the QC samples and RSD>30% QC samples were removed. To obtain a full list of all the metabolites detected in this study, all the metabolic date obtained from the positive and negative modes of LC-MS/MS and GC-TOF-MS were merged as a single file. The duplicate metabolites were screened based on their scores as calculated by in-house algorithms, and the metabolites with the highest score were kept in a combined file (Biotree Biomedical Technology Co., Ltd).

2.6. Statistical analyses

Metabolomics profiles were statistically analyzed via the online analysis software MetaboAnalyst 5.0 (http://www.metaboanalyst.ca, Chong et al., 2019). Before the statistical analysis, the metabolomic data were normalized by median and auto-scaling. The statistically significantly changed metabolites between the pre- and post-pubertal molt groups were identified via Student's *t*-test. Multivariate principal component analysis (PCA) and orthogonal projection to latent structures discriminant analysis (oPLS-DA) were conducted to discriminate between the pre- and post-pubertal molt groups. A permutation test (1000 times) was performed to validate the quality of the oPLS-DA model. The variable importance in the projection (VIP) score of the first principal component in oPLS-DA was calculated to explain the importance of different metabolites (Li et al., 2020). Two selection criteria were used to propose significantly changed metabolites after pubertal molt: (1)
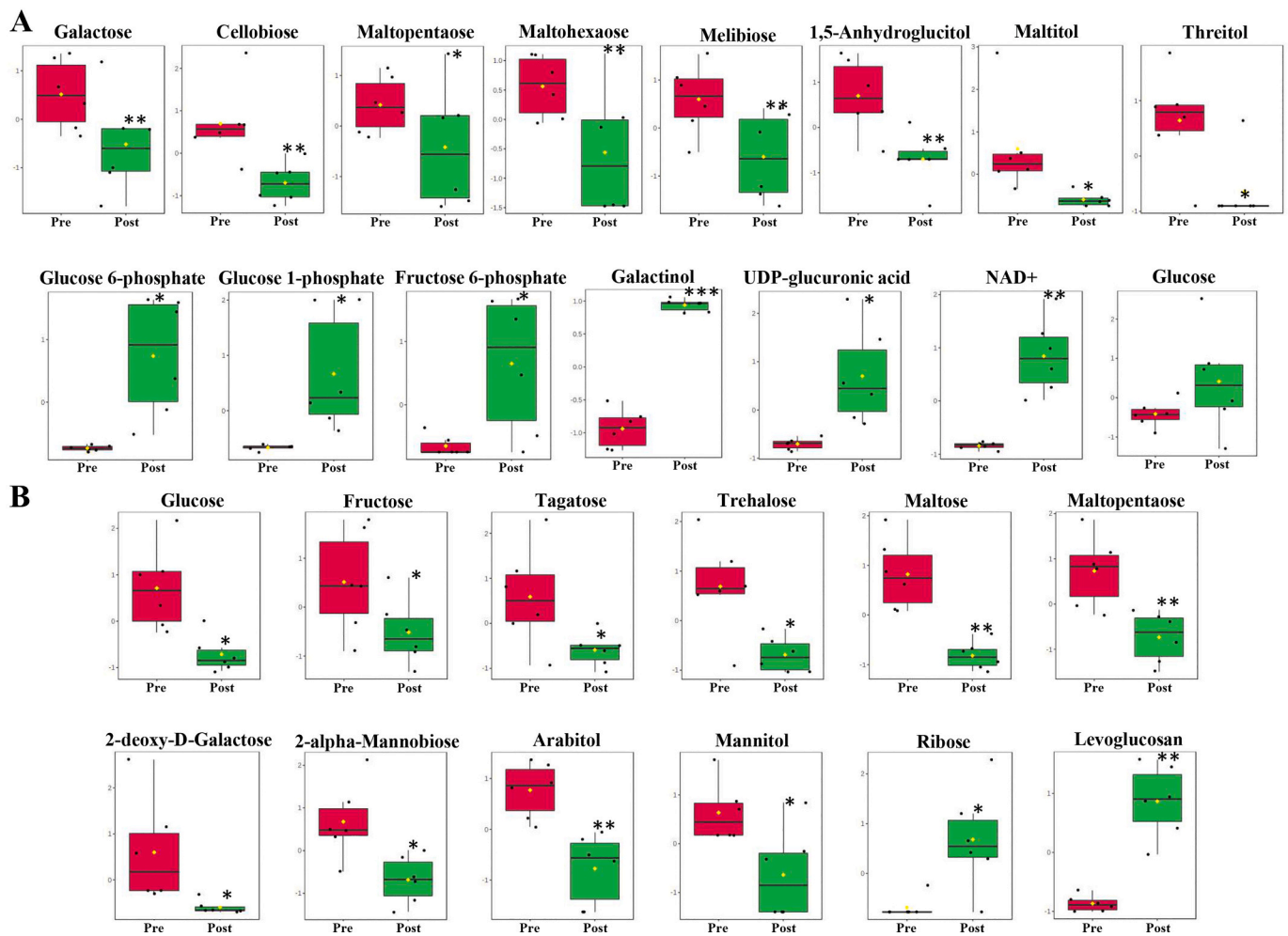
Fig. 2. The most obviously changed carbohydrates in the hepatopancreas (A) and ovary (B) between the pre- and post-pubertal molting groups. Pre, the pre-pubertal molt group; Post, the post-pubertal molt group. *, significantly different (p value <0.05); **, very significantly different (p value <0.01); ***, extremely significantly different (p value <0.001).

statistical significance (p value <0.05), (2) VIP score > 1.

Metabolite pathway analysis (MetPA) was performed based on pathway-associated metabolite sets. The parameters in MetPA were set as follows: the enrichment method, topology analysis, and pathway library were set as global test, relative-betweeness centrality, and *Drosophila melanogaster* (fruit fly, KEGG) (Chong et al., 2019).

Receiver operating characteristics (ROCs) and areas under the ROC curve (AUC) were calculated to explore the discriminative capability of different metabolites via MetaboAnalyst 5.0. Multivariate exploratory ROC analysis, including feature selection, model building, and performance evaluation, were generated by Monte-Carlo cross-validation (MCCV). Partial least squares–discriminant analysis (PLS-DA) for classification and "PLS-DA built-in" analysis for feature ranking were generated as a multivariate algorithm to perform biomarker identification (Chong et al., 2019).

3. Results

3.1. Overview of metabolomic profiles of hepatopancreas and ovary

In the present study, common sets of 873 and 641 metabolites were identified in the hepatopancreas and ovary via the metabolomics approach, respectively. Several major metabolite categories have been identified, including lipids (230 and 159 metabolites), carbohydrates (37 and 31 metabolites), amino acids (22 and 26 metabolites),

nucleotides (22 and 21 metabolites), and vitamins (5 and 5 metabolites), in the hepatopancreas and ovary, respectively (Fig. 1A, B). In the multivariate analysis of metabolomic profiles, both the PCA (PC1 = 29.6%, PC2 = 12.7%) and oPLS-DA (T score [1] = 28%, Orthogonal T score [1] = 11.4%) score plots of metabolomic profiles in the hepatopancreas displayed clear separations between the pre- and post-pubertal molt groups (Fig. 1E, F). The PCA score plot (PC1 = 25.6%, PC2 = 14.5%) of the metabolomic profiles of the ovary showed a less clear separation between the pre- and post-pubertal molt groups (Fig. 1G); however, the oPLS-DA score plot (T score [1] = 20.7%, Orthogonal T score [1] = 15.2%) provided much better discrimination (Fig. 1H). The permutation test of the oPLS-DA model obtained a Q^2 of 89.1% ($p = 0.003$, 3/1000) and an R^2Y of 99.5% ($p = 0.005$, 5/1000) for the metabolomic profiles in the hepatopancreas (Supplementary Fig. 3A), and a Q^2 of 81.5% ($p = 0.003$, 3/1000) and R^2Y of 99.9% ($p = 0.003$, 3/1000) for the metabolomic profiles in the ovary, respectively (Supplementary Fig. 3B). This indicates that the oPLS-DA models for both hepatopancreas and ovary had good descriptive and predictive capabilities.

3.2. Significantly changed metabolites and metabolites pathway analysis (MetPA)

Compared with the pre-pubertal molt group, 251 (28.75%) and 145 (22.93%) metabolites were recognized to be significantly changed in the
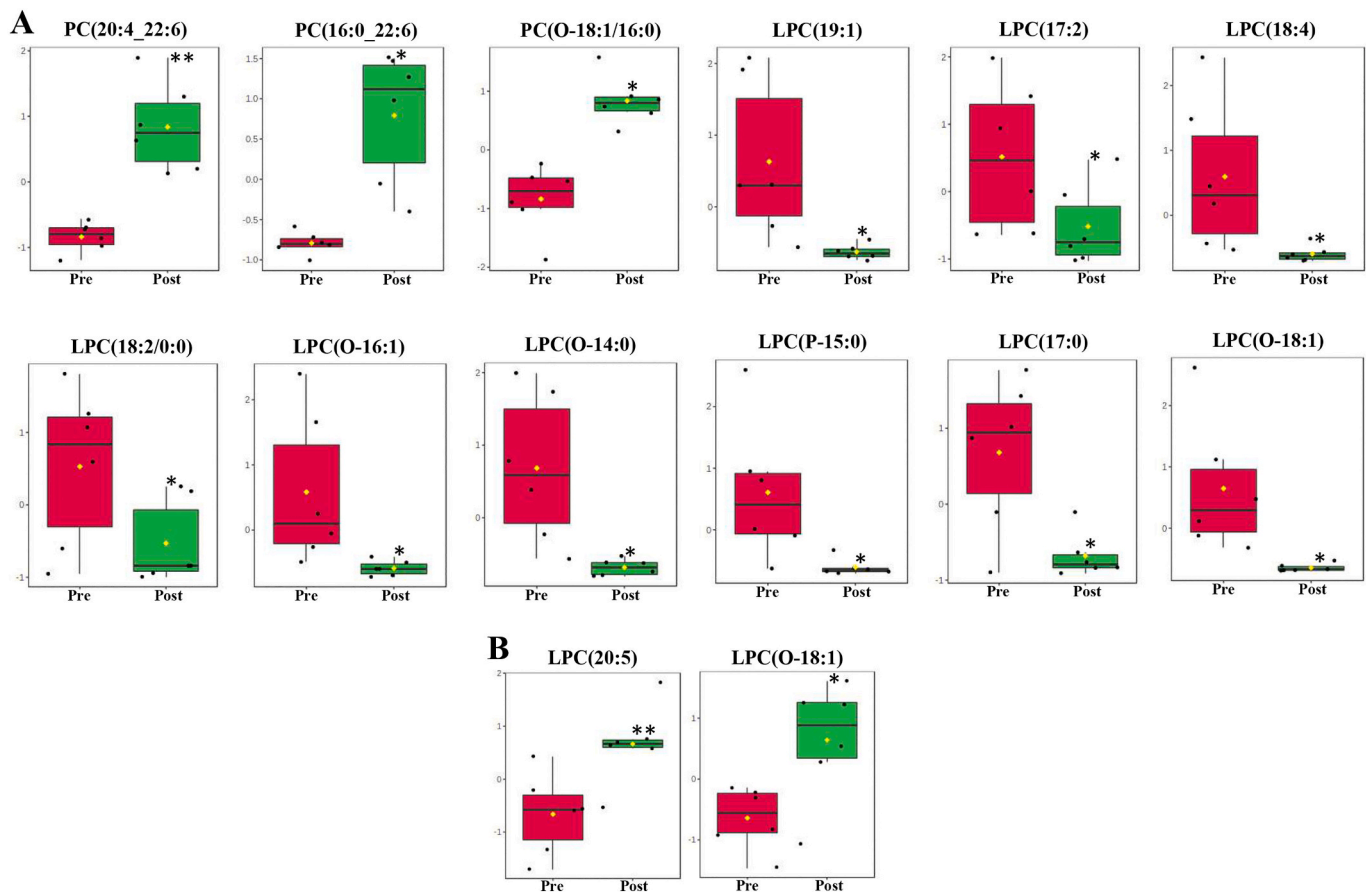
Fig. 3. The significantly changed amino acids in the hepatopancreas (A) and ovary (B) between the pre- and post-pubertal molting groups. Pre, the pre-pubertal molt group; Post, the post-pubertal molt group. *, significantly different (*p* value <0.05); **, very significantly different (*p* value <0.01); ***, extremely significantly different (*p* value <0.001).

hepatopancreas and ovaries postmolt, respectively. The numbers of significantly changed carbohydrates, lipids, amino acids, nucleotides, and vitamins in the hepatopancreas and ovary are listed in Fig. 1C, D, respectively. In the hepatopancreas, the MetPA of the remarkably changed metabolites revealed that 27 pathways were notably enriched post-pubertal molt, which were separated into eight KEGG pathway classes (Table 1). Among them, 11, 7 and 4 pathways were involved in carbohydrate, amino acid and other amino acid, and lipid metabolisms, respectively (Table 1). In the ovary, 25 pathways were remarkably enriched in the significantly changed metabolites postmolt, and these pathways were assigned into seven KEGG pathway classes (Table 2). In total, 7, 12 and 1 pathways were related to carbohydrate, amino acid and other amino acid, and lipid metabolisms, respectively (Table 2). Among the significantly enriched pathways, 5, 6, and 1 pathways involved in carbohydrate, amino acid and other amino acid, and lipid metabolisms were the same between the hepatopancreas and ovary, respectively. Besides this, pantothenate and CoA biosynthesis, pyrimidine metabolism, and aminoacyl-tRNA biosynthesis were significantly modulated in both hepatopancreas and ovary postmolt.

In addition, five carbohydrate metabolic pathways were significantly enriched in both the hepatopancreas (45.45% of all the carbohydrate metabolic pathways) and ovary (71.43% of them), indicating that the carbohydrate metabolism was mainly modulated in the hepatopancreas. Moreover, six significantly enriched amino acid and other amino acid metabolic pathways were remarkably enriched in both the hepatopancreas (85.71% of all the amino acid and other amino acid metabolic pathways) and ovary (50% of them), suggesting that the metabolism of amino acids and other amino acids was generally modulated in the ovary. Furthermore, lipid metabolic pathways were obviously affected

in the hepatopancreas, but only slightly affected in the ovary, postmolt.

3.3. Obviously changed carbohydrates in hepatopancreas and ovary

Compared with the pre-pubertal molt group, 13 carbohydrates in the hepatopancreas were recognized to be significantly changed postmolt (Fig. 2A). The levels of glucose 6-phosphate, glucose 1-phosphate, fructose 6-phosphate, UDP-glucuronic acid, and galactinol were significantly increased, and the glucose level was comparatively increased, postmolt. Meanwhile, another eight carbohydrates were significantly decreased, including galactose, cellobiose, maltopentaose, maltohexaose, melibiose, 1,5-anhydroglucitol, maltitol and threitol (Fig. 2A, Supplementary Table 4).

On the other hand, 12 carbohydrates were remarkably changed in the ovary postmolt; 10 of them were significantly decreased in abundance postmolt, including glucose, fructose, tagatose, trehalose, maltose, maltopentaose, 2-deoxy-D-galactose, 2-alpha-mannobiose, arabitol, and mannitol (Fig. 2B, Supplementary Table 5). Moreover, the levels of glucose 6-phosphate, glucose 1-phosphate, and fructose 6-phosphate were slightly increased in the ovary postmolt (Supplementary Table 1).

The levels of glucose 6-phosphate, glucose 1-phosphate and fructose 6-phosphate were significantly increased in the hepatopancreas and slightly increased in the ovary postmolt, suggesting glycolysis was dramatically upregulated in hepatopancreas. However, the glucose levels in the hepatopancreas were slightly increased and significantly decreased in the ovary, which continuously stimulated glycolysis for energy supply in the hepatopancreas but reduced glycolysis in the ovary. Besides this, the significant increase in NAD^+ levels in the
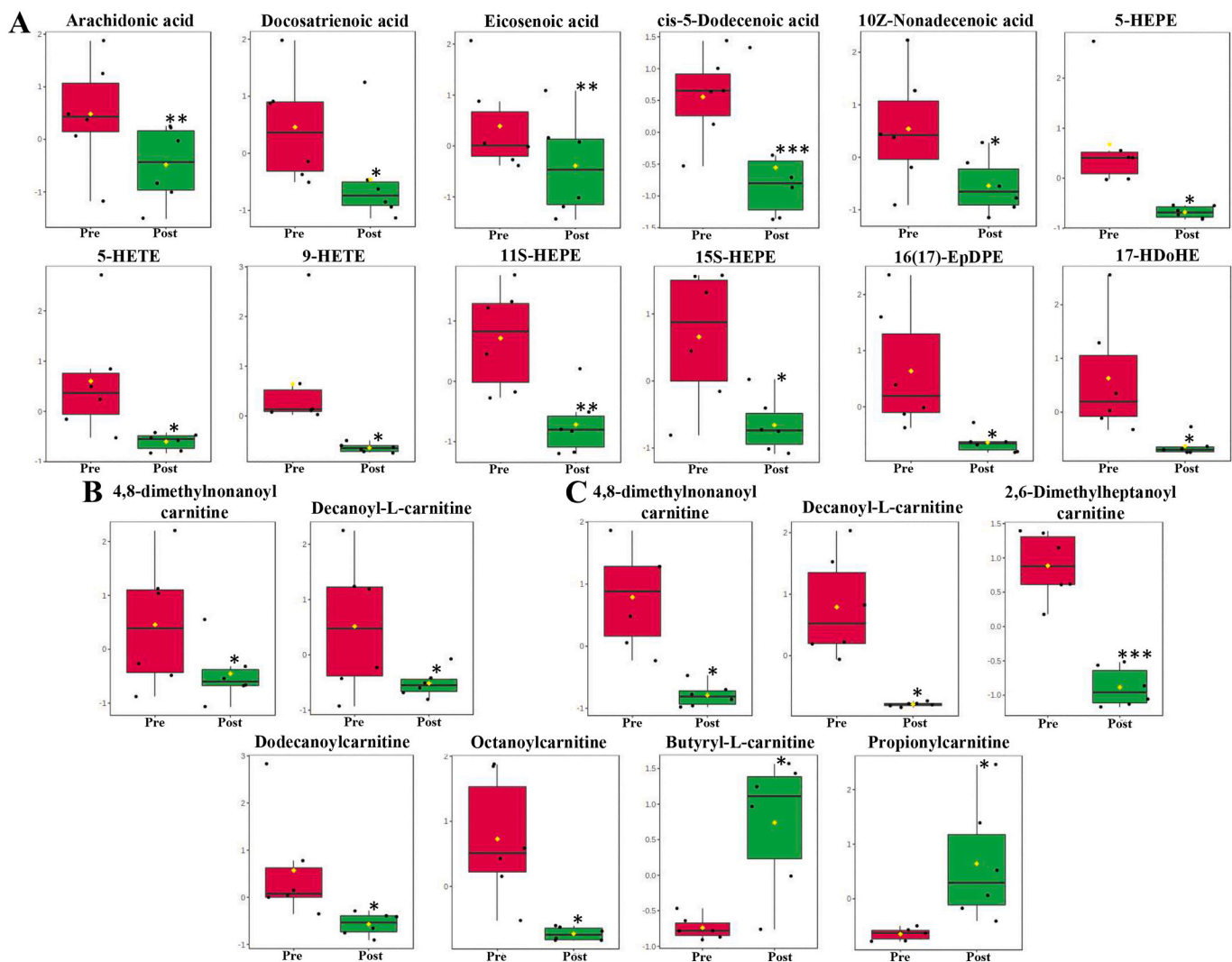
Fig. 4. The most significantly changed vitamins (A, B) and nucleotides (C, D) in the hepatopancreas (A, C) and ovary (B, D) between the pre- and post-pubertal molting groups. Pre, the pre-pubertal molt group; Post, the post-pubertal molt group. *, significantly different (*p* value <0.05); **, very significantly different (*p* value <0.01); ***, extremely significantly different (*p* value <0.001).

hepatopancreas also suggests the energy supply derived from the glycolysis of carbohydrates was stimulated (Fig. 2A).

3.4. Significantly changed lipids in hepatopancreas and ovary

Compared with the pre-pubertal molt group, in the hepatopancreas, 65 lipids were identified to be significantly changed postmolt, including 16 glycerophospholipids (GP) and 33 fatty acids (FA). Among the 16 GP, 3 glycerophosphocholines (GPC) were significantly increased in level postmolt, including PC(20:4_22:6), PC(16:0_22:6), and PC(O-18:1/16:0) (Fig. 3A). PC(20:4_22:6) and PC(16:0_22:6) were diacyl-GPC (GP0101), and PC(O-18:1/16:0) was 1-alkyl,2-acyl-GPC (GP0102) (LIPID MAPS, https://www.lipidmaps.org/). Moreover, another nine GPC were notably decreased in content, including five monoacyl-GPC (GP0105), three 1Z-alkenyl-GPC (GP0107), and one monoalkyl-GPC (GP0106) (Fig. 3A, Supplementary Table 4). Of the 33 FA, the unsaturated fatty acids (FA0103) (unsaturated FA, 12/33) were the most abundant FA subclasses identified in the hepatopancreas. In total, 12 unsaturated FA were significantly reduced in abundance in the hepatopancreas postmolt (Fig. 4A, Supplementary Table 4). Moreover, the levels of two fatty acyl carnitines (FA0707), namely 4,8-dimethylnonanoyl carnitine and decanoyl-L-carnitine, were significantly reduced in the hepatopancreas postmolt (Fig. 4B, Supplementary Table 4).

In the ovary, 23 lipids were remarkably changed postmolt, resulting in three GP and 15 FA. The levels of two monoacyl-GPC, namely LPC (20:5) and LPC(O-18:1), were significantly increased in the ovary postmolt (Fig. 3B, Supplementary Table 5). Fatty acyl carnitines (FA0707) (7/15) were identified to be the most abundant FA subclass in the ovary (Fig. 4C, Supplementary Table 5). Among these, the levels of five medium-chain fatty acyl carnitines were significantly decreased, including 4,8-dimethylnonanoyl carnitine (C11-carnitine), decanoyl-L-carnitine (C10-carnitine), 2,6-Dimethylheptanoyl carnitine (C9-carnitine), dodecanoylcarnitine (C12-carnitine), and octanoylcarnitine (C8-carnitine), but the levels of short-chain fatty acyl carnitines, namely butyryl-L-carnitine (C4-carnitine) and propionylcarnitine (C3-carnitine), were remarkably increased postmolt. Besides this, only one unsaturated FA was notably decreased in content in the ovary postmolt (14,15-Leukotriene C4). In addition, eight monoacyl−/monoalkyl−/1Z-alkenyl−GPC and four unsaturated FA were present in both the hepatopancreas and the ovary. The levels of these monoacyl−/monoalkyl−/1Z-alkenyl−GPC and unsaturated FA were decreased in the hepatopancreas, but increased in the ovary, postmolt (Supplementary Tables 2, 3). For example, the level of LPC(O-18:1) was significantly decreased in the hepatopancreas but remarkably increased in the ovary (Fig. 3A, B, Supplementary Table 2). The levels of arachidonic acid (AA), 5-HEPE, 15S-HEPE, and 17-HDoHE were significantly decreased in the
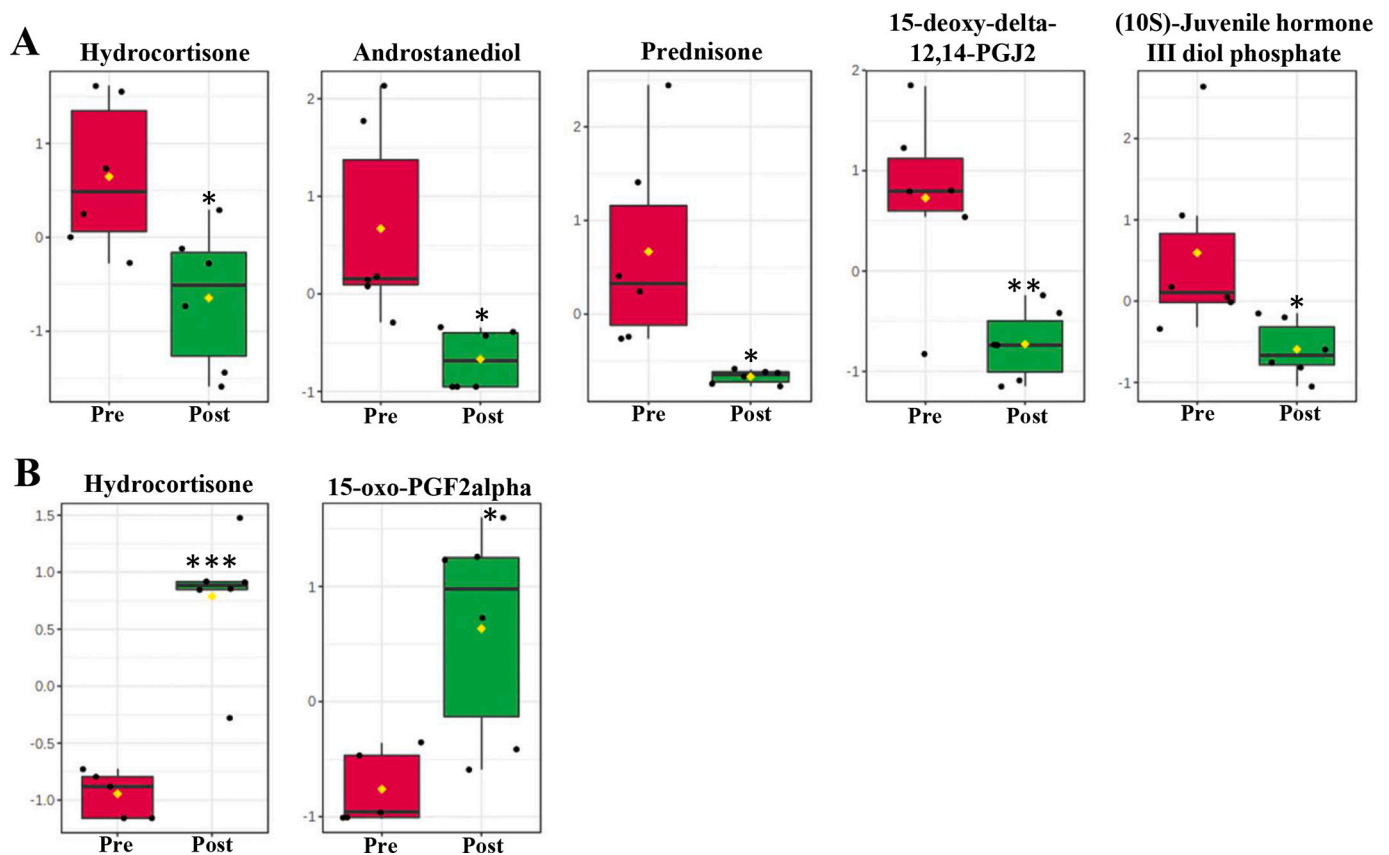
Fig. 5. The significantly changed glycerophospholipids in hepatopancreas (A) and ovary (B) between the pre- and post-pubertal molting groups. Pre, the pre-pubertal molt group; Post, the post-pubertal molt group. *, significantly different (p value <0.05); **, very significantly different (p value <0.01); ***, extremely significantly different (p value <0.001).

hepatopancreas, but increased in the ovary (Fig. 4A; Supplementary Table 3).

3.5. Significantly changed hormones (or hormone analogs) in hepatopancreas and ovary

In the hepatopancreas, the levels of five hormones (or hormone analogs) were identified to be significantly decreased postmolt, including hydrocortisone, androstanediol, prednisone, 15-deoxy-delta-12,14-PGJ2, and 10S-Juvenile hormone III diol phosphate (Fig. 5A, Supplementary Table 4). Meanwhile, the contents of two hormones (or hormone analogs) were significantly increased postmolt in the ovary, namely, hydrocortisone and 15-oxo-PGF2alpha (Fig. 5B, Supplementary Table 5). Furthermore, the abundance of hydrocortisone was identified to be significantly decreased in the hepatopancreas, but was remarkably increased in the ovary post-pubertal molt (Fig. 5A, B).

3.6. Significantly changed amino acids, vitamins, and nucleotides in hepatopancreas and ovary

In the hepatopancreas, compared with the pre-pubertal molt group, nine amino acids, three vitamins and three nucleotides were significantly changed postmolt. Among the nine amino acids, the levels of six were notably decreased, but another three were remarkably increased postmolt (Fig. 6A, Supplementary Table 4). The levels of three vitamins, namely, pantothenic acid, myo-inositol, and ascorbate, were significantly increased postmolt (Fig. 7A, Supplementary Table 4). Meanwhile, the deoxycytidine level was significantly decreased, and the levels of cytosine and AMP were remarkably increased in the hepatopancreas, postmolt (Fig. 7C, Supplementary Table 4).

In the ovary, eight amino acids, two vitamins and two nucleotides

were identified to be significantly changed postmolt. The levels of four amino acids (valine, cysteine, histidine and isoleucine, Fig. 6B, Supplementary Table 5) and one nucleotide (Inosine monophosphate, IMP, Fig. 7D, Supplementary Table 5) were remarkably decreased. Meanwhile, the levels of four amino acids (tryptophan, o-phosphoserine, ornithine, and citrulline, Fig. 6B), two vitamins (pantothenic acid and myo-inositol, Fig. 7B), and one nucleotide (guanosine, Fig. 7D) were significantly increased postmolt.

3.7. Receiver operating characteristics (ROC) analysis

In the hepatopancreas, classical univariate ROC analysis revealed that 61 metabolites obtained an AUC of 1.0 (AUC, area under the curve; upregulated/downregulated = 18/43). ROC analysis revealed that the major potential metabolic biomarkers in the hepatopancreas decreased in content (29.5% up vs. 70.5% down). The multivariate ROC curves from all the models based on cross-validation performance indicated that ROC models with more than 10 features (metabolites) obtained the highest AUC (1.0, Fig. 8A), and the models with 100 features (metabolites) attained the best predictive accuracy (99.5%, Fig. 8C).

In the ovary, 51 metabolites reached an AUC of 1.0 (upregulated/downregulated = 23/28) post-pubertal molting. Meanwhile, the identified potential metabolic biomarkers (45.1% up vs. 54.9% down) indicated the up- and downregulated metabolites were evenly matched in the ovary. The multivariate ROC curves indicate that the ROC models with more than 25 features (metabolites) obtained the highest AUC (1.0, Fig. 8B), and the model with 100 features (metabolites) attained the best predictive accuracy (98.8%, Fig. 8D).

Based on classical univariate and multivariate ROC curve analysis, the first ten metabolites (the first 10% of features in the ROC model with the best predictive accuracy) in the hepatopancreas and ovary were
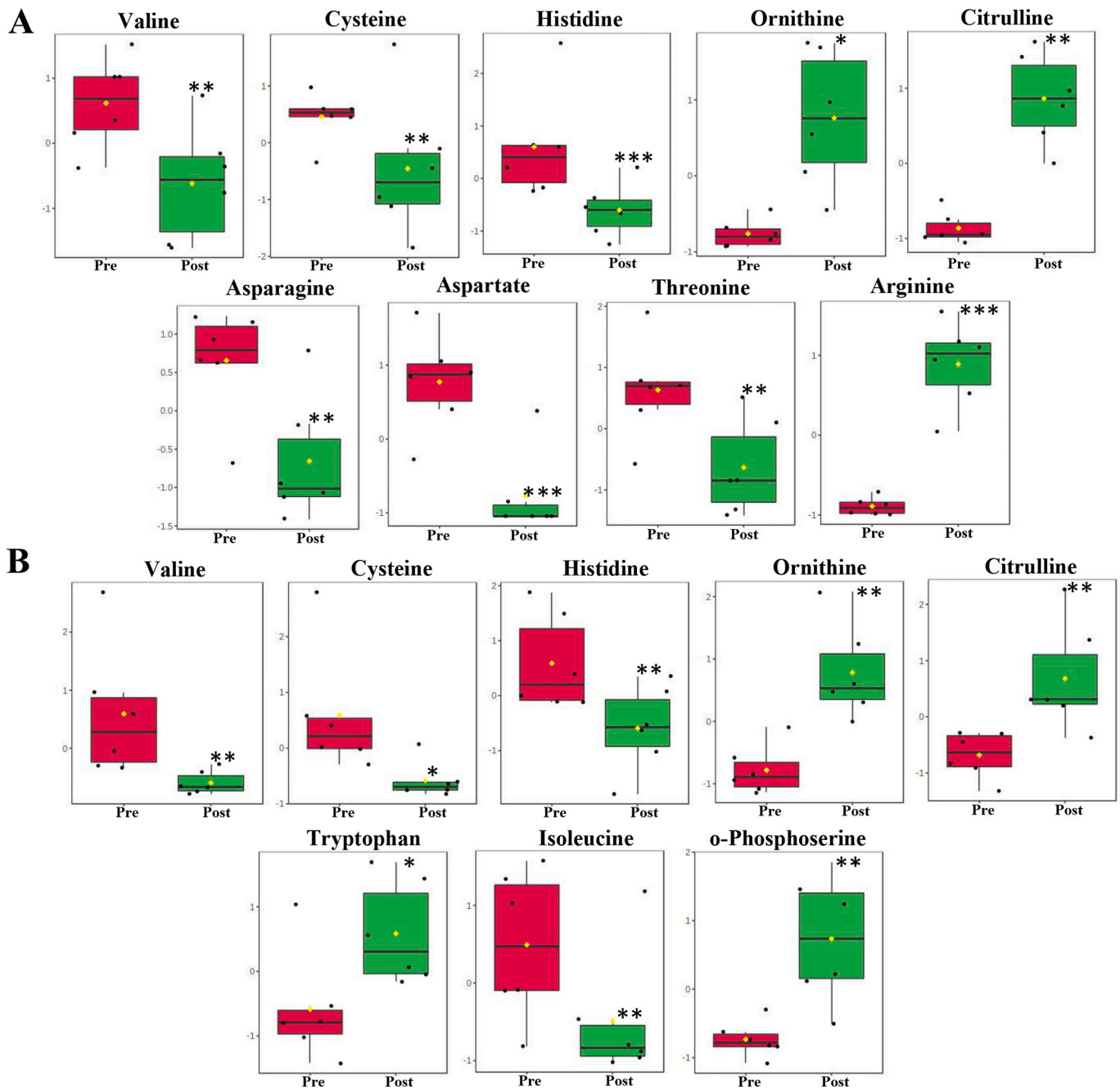
Fig. 6. The most significantly changed unsaturated fatty acids in the hepatopancreas (A), and fatty acyl carnitines in the hepatopancreas (B) and ovary (C) between the pre- and post-pubertal molting groups. Pre, the pre-pubertal molt group; Post, the post-pubertal molt group. *, significantly different (*p* value <0.05); **, very significantly different (*p* value <0.01); ***, extremely significantly different (*p* value <0.001).

identified as the best predictive biomarkers with the highest selected frequency and average importance in the biomarker panel, respectively (Fig. 8E, F).

4. Discussion

For most female crustaceans, pubertal molt is a natural and important process for mating and subsequent ovarian development (Sánchez-Paz et al., 2007). Molting requires a significant amount of energy (Niu et al., 2012). However, a period of starvation (fasting) occurs during pubertal molting, which makes internal nutrients critical for survival and the initiation of ovarian development. Plenty of previous studies have indicated that the energy reserves involved in short-term starvation, a state that is similar to fasting during molting, vary depending on species, development stage, and even season (Cherel et al., 1992; Sánchez-Paz et al., 2007; Sugumar et al., 2013). The information on energy reserves and the nutrients utilized for survival and the initiation of ovarian development in pubertal molting is not clear. The hepatopancreas and ovary are two important organs involved in pubertal molting, and changes in the metabolite profiles of these organs may elucidate the dynamics of internal nutrient utilization during pubertal molting.

MetPA revealed that the metabolism of carbohydrates and lipids in the hepatopancreas was significantly affected (Table 1). Moreover, the significant increases in glucose 6-phosphate, glucose 1-phosphate, and fructose 6-phosphate indicate that glycolysis was promoted in the
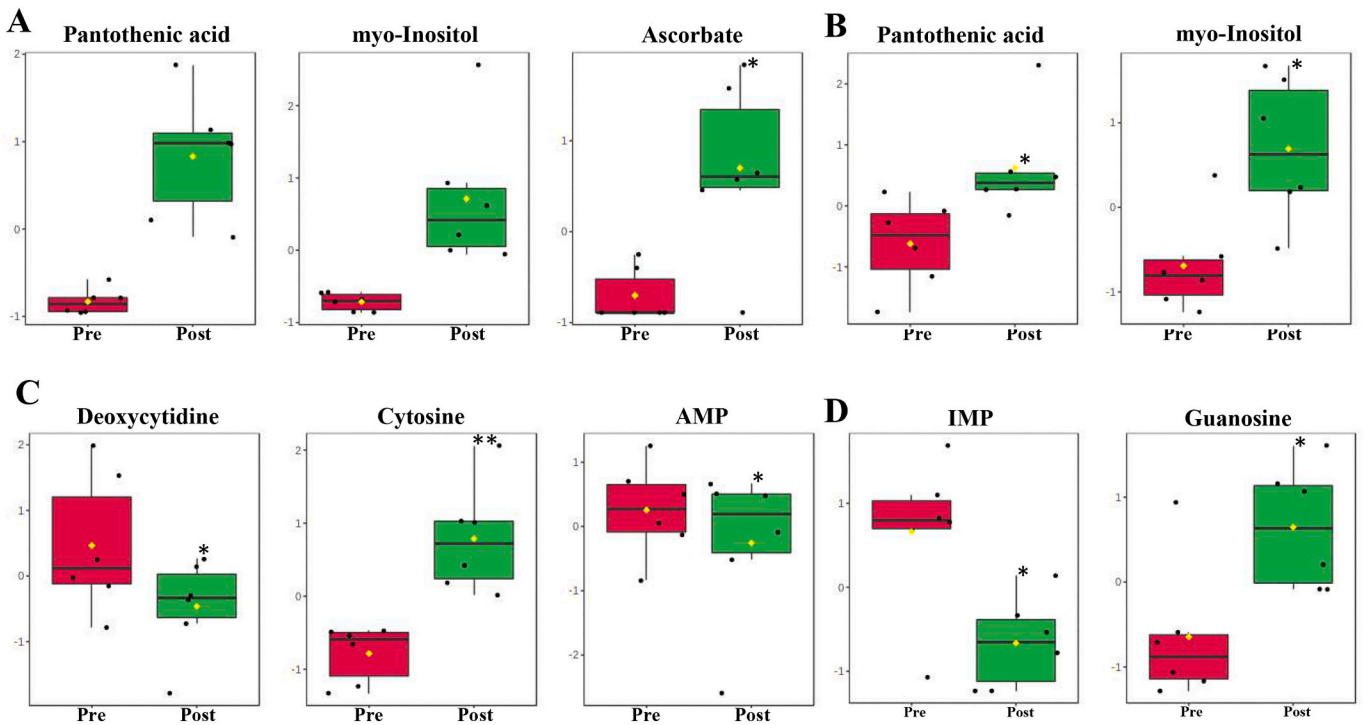
Fig. 7. The significantly changed hormones in the hepatopancreas (A) and ovary (B) between the pre- and post-pubertal molting groups. Pre, the pre-pubertal molt group; Post, the post-pubertal molt group. *, significantly different (*p* value <0.05); **, very significantly different (*p* value <0.01); ***, extremely significantly different (*p* value <0.001).
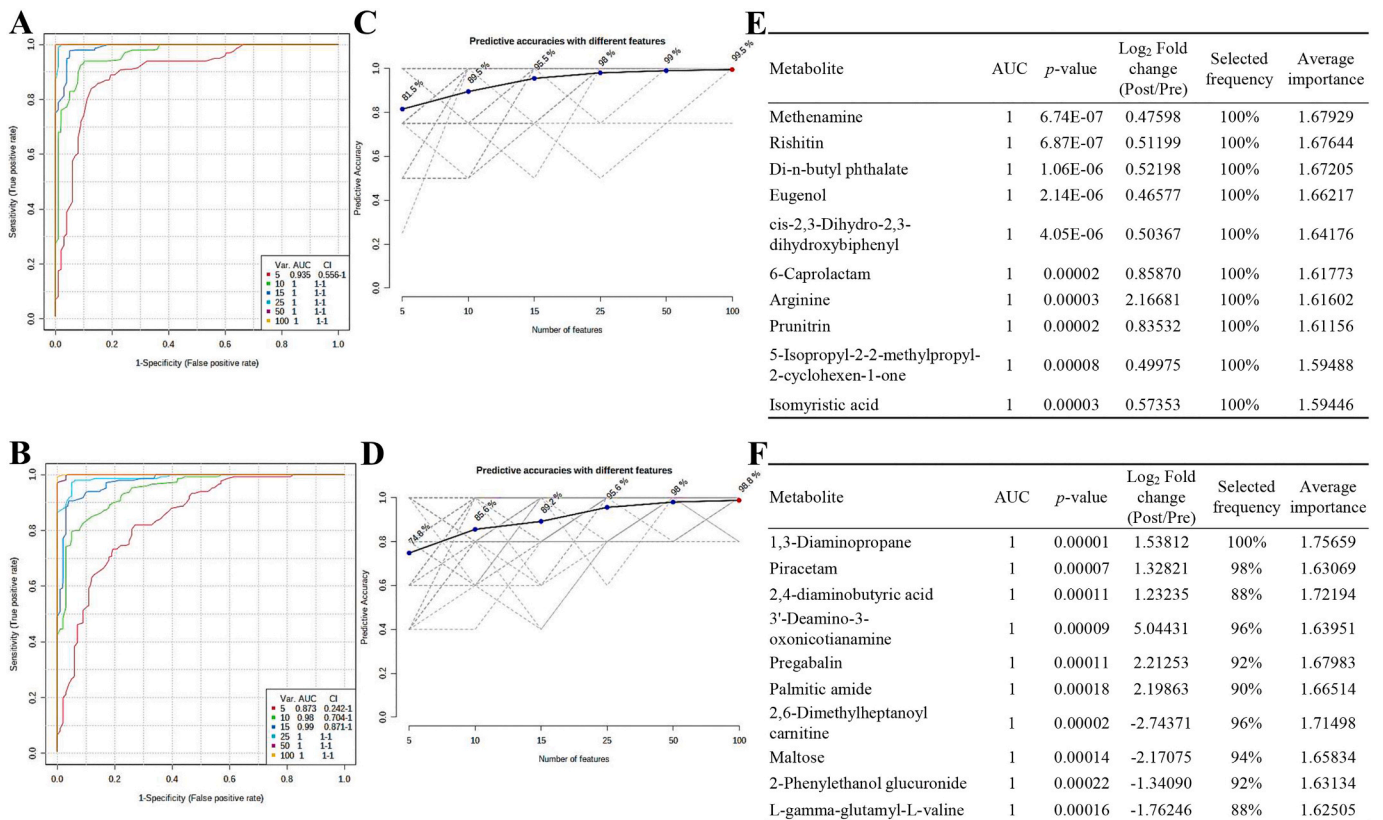

Fig. 8. Overview of the multiple ROC analyses and the potential biomarkers identified in the metabolomic profile from the hepatopancreas (A, C, E) and ovary (B, D, F) of *S. paramamosain* during pubertal molting. A and C, multiple ROC curves; B and D, predictive accuracies with different features; C and F, potential metabolite biomarkers for pubertal molting.

hepatopancreas postmolt. Meanwhile, the increase in glucose level in the hepatopancreas, indicating glycogenolysis, was stimulated, and free glucose was released in the hepatopancreas postmolt (Fig. 2A). Therefore, carbohydrates may be the major supplier of energy that is consumed via glycolysis in the hepatopancreas under fasting conditions.

When fasting occurs during molting, crustaceans activate their lipid and glycogen metabolism in the hepatopancreas, with the lipid metabolism dominating (Teshima et al., 1977; Huang et al., 2020). Lipids are a major source of energy and essential nutrients in marine crustaceans (Wen et al., 2001). In this study, 65 lipids were recognized to be significantly changed in the hepatopancreas postmolt, including 12 glycerophosphocholines (GPC) and 12 unsaturated fatty acids (UFA). GPC are important phospholipids, which enhance lipid emulsification and transport to improve lipid deposition and energy utilization (Han et al., 2018; Fang et al., 2021). UFA play vital roles in the development of marine crustaceans as sources of energy and as structural components of membranes (Suprayudi et al., 2004). In the hepatopancreas of *Homarus americanus*, triacylglycerides are cleaved into diacylglycerols, monoacylglycerols, and free fatty acids (Kumar et al., 2018), and monoglycerides and free fatty acids are either catabolized by β-oxidation or transported to other tissues or cells for storage (Glencross, 2009). In the hepatopancreas, the significant changes in GPC and UFA were possibly related to energy supply or lipid output under fasting conditions during pubertal molting. Therefore, the significant changes in GPC and unsaturated FA in the hepatopancreas may have been due to their consumption as another energy source in the hepatopancreas, or their exporting to other tissues during fasting in the pubertal molt stage.

In the ovary, the levels of glucose 6-phosphate and fructose 6-phosphate were slightly increased, indicating glycolysis may have been upregulated postmolt. However, different from the changes in the hepatopancreas, the significant reduction in 10 carbohydrates, especially glucose, suggests there was an insufficient supply of carbohydrates in the ovary, which possibly inhibited the further upregulation of glycolysis under fasting conditions during pubertal molting (Fig. 2B, Supplementary Table 1). Moreover, as the most abundant fatty acids in the ovary, five medium-chain fatty acyl carnitines were significantly decreased. Meanwhile, two short-chain fatty acyl carnitines were remarkably increased in content postmolt (Fig. 4C), suggesting that fatty acyl carnitines play crucial roles in the ovary during pubertal molting. The main pathway of fatty acid catabolism is β-oxidation in the mitochondrial matrix, but mitochondrial membranes are impermeable to acyl-CoAs, and so a carnitine shuttle exists to convey fatty acyls across the mitochondrial membranes in the form of fatty acyl carnitines (Lam et al., 2020). Moreover, short-chain fatty acyl carnitines, such as propionylcarnitine and butyryl-L-carnitine, are usually derived from the latter stages of fatty acid oxidation (Lam et al., 2020). Thus, the significant reduction in medium-chain fatty acyl carnitines and the increase in short-chain fatty acyl carnitines suggests β-oxidation was stimulated to improve energy supply in the ovary, and the fatty acyl carnitines may have been consumed as the major energy reserves in the ovary postmolt.

On the other hand, pubertal molting initiates ovarian development, which is expensive in terms of energy and nutrient expenditure. Internal resources are tightly partitioned between growth and reproduction (Capparelli and Flores, 2011). Furthermore, ovarian development relies on exogenous vitellogenesis and lipids from the hepatopancreas (Yao et al., 2008). Wen et al. (2001) also reported the movement of hepatopancreatic lipids to the ovaries during ovarian maturation in *Eriocheir sinensis*. However, the vital metabolites that must accumulate for the initiation of ovarian development are still unclear. In this study, eight GPC and four UFA were found to be present in both the hepatopancreas and ovary. The levels of all these lipids were decreased in the hepatopancreas but increased in the ovary (Supplementary Tables 2, 3). This suggests monoacyl−/monoalkyl−/1Z-alkenyl−GPC and UFA were exported from the hepatopancreas and accumulated in the ovary. GPC enhances lipid emulsification and transport in order to improve lipid deposition and energy utilization (Han et al., 2018; Fang et al., 2021).

UFA, especially arachidonic acid (AA), eicosapentaenoic acid (EPA), and docosahexaenoic acid (DHA), play multiple roles in crustacean reproduction as energy suppliers or cellular components (Glencross, 2009; Taipale et al., 2011; Ginjupalli et al., 2015; Li et al., 2021). 5-HEPE and 15S-HEPE are metabolic products of EPA, and 17-HDoHE is a hydroxy DHA. In this study, the levels of AA, 5-HEPE, 15S-HEPE, and 17-HDoHE were significantly increased in the ovary, suggesting their possible recruitment. Besides this, the hepatopancreas is an important site for the synthesis of steroid hormones, which fulfill important functions during pubertal molting and the ensuing ovarian development (Yang et al., 2005; Jiang et al., 2009). In this investigation, hydrocortisone was significantly reduced in the hepatopancreas but was remarkably increased in the ovary postmolt (Fig. 5A, B), which may suggest that the initiation of ovarian development requires hormones from the hepatopancreas. As a glucocorticoid analog, hydrocortisone regulates the reproductive activity and metabolism of pond snails *Lymnaea stagnalis*, as an active inducer of the initial stages of blastogenesis (Kudikina, 2011). Taken together, the accumulation of GPC, UFA, and other specific hormones (such as hydrocortisone) in the ovary may play an important role in the initiation of ovarian development, such as energy supply, cellular component construction, and reproductive regulation. This is an interesting point that deserves more attention in further research. In addition, the changes in amino acids and vitamins in the hepatopancreas and ovary were similar, suggesting amino acids and vitamins might be essential to basic physiological functions in multiple organs during pubertal molting. For example, osmoregulation is another vital physiological process during pubertal molting, and free amino acids have been reported to be important osmoregulatory substances in *S. paramamosain* (Yao et al., 2020).

5. Conclusions

In conclusion, a comprehensive investigation was conducted on the metabolomic profiles of the hepatopancreas and ovaries of female mud crabs during pubertal molting. The major carbohydrates, lipids, amino acids, nucleotides, vitamins, and hormones were identified in the hepatopancreas and ovary, respectively. Carbohydrates were found to be the major energy supplier in the hepatopancreas during pubertal molting. Meanwhile, fatty acyl carnitines were found to be consumed via β-oxidation for energy supply in the ovary. Moreover, the various glycerophosphocholines, unsaturated fatty acids, and hormones were exported from the hepatopancreas and accumulated in the ovary, which may contribute to the initiation of ovarian development during pubertal molting. In addition, the changes in amino acids and vitamins in the hepatopancreas and ovary were similar, suggesting amino acids and vitamins may be essential to basic physiological functions in multiple organs during pubertal molting. The present study not only provides a comprehensive review of the major energy reserves consumed during pubertal molting, but also preliminarily identifies the vital nutrients involved in the initiation of ovarian development. Further research will focus on the regulatory mechanisms involved in the deployment and utilization of internal nutrients, and will develop a proper model of nutrition supply in female mud crabs before pubertal molting in the aquaculture industry.

Declaration of Competing Interest

The authors declare that they have no known competing financial interests or personal relationships that could have appeared to influence the work reported in this paper.

Acknowledgments

Appendix A. Supplementary data

Supplementary data to this article can be found online at https://doi.org/10.1016/j.aquaculture.2021.737736.

References

Alfaro, A.C., Young, T., 2018. Showcasing metabolomic applications in aquaculture: a review. Rev. Aquac. 10 (1), 135–152.

Barclay, M.C., Dall, W., Smith, D.M., 1983. Changes in lipid and protein during starvation and the moulting cycle in the tiger prawn, *Penaeus esculentus* Haswell. J. Exp. Mar. Biol. Ecol. 68, 229–244.

Bowser, P.R., Rosemark, R., 1981. Mortalities of cultured lobsters, Homarus, associated with a molt death syndrome. Aquaculture 23, 11–18.

Capparelli, M.V., Flores, A.A.V., 2011. Environmentally driven shift between alternative female morphotypes in the mottled shore crab. Zoology 114, 276–283.

Chan, S.M., Rankin, S.M., Keeley, L.L., 1988. Characterization of the molt stages in *Penaeus vannamei*: setogenesis and hemolymph levels of total protein, ecdysteroids, and glucose. Biol. Bull. 175 (2), 185–192.

Chang, E.S., Mykles, D.L., 2011. Regulation of crustacean molting: a review and our perspectives. Gen. Comp. Endocrinol. 172 (3), 323–330.

Cherel, Y., Robin, J.P., Heitz, A., Calgari, C., Maho, L.Y., 1992. Relationships between lipid availability and protein utilization during prolonged fasting. J. Comp. Physiol. B. 162 (4), 305–313.

China Fishery Statistical Yearbook, 2019.

Chong, J., Wishart, D.S., Xia, J., 2019. Using MetaboAnalyst 4.0 for comprehensive and integrative metabolomics data analysis. Curr. Protoc. Bioinformatics 68, e86.

Corteel, M., Dantas-Lima, J.J., Wille, M., Alday-Sanz, V., Pensaert, M.B., Sorgeloos, P., Nauwynck, H.J., 2009. Molt stage and cuticle damage influence white spot syndrome virus immersion infection in penaeid shrimp. Vet. Microbiol. 137 (3–4), 209–216.

Fang, F., Yuan, Y., Jin, M., Shi, B., Zhu, T., Luo, J., Zhou, Q., 2021. Hepatopancreas transcriptome analysis reveals the molecular responses to different dietary n-3 PUFA lipid sources in the swimming crab *Portunus trituberculatus*. Aquaculture 543, e737016.

Fazhan, H., Waiho, K., Norfaizza, W.I.W., Megat, F.H., Ikhwanuddin, M., 2017. Assortative mating by size in three species of mud crabs, genus *Scylla De Haan*, 1833 (*Brachyura: Portunidae*). J. Crustac. Biol. 37, 654–660.

Gao, T., Xu, Y., Wang, K., Deng, Y., Yang, Y., Lu, Q., Xu, Z., 2018. Comparative LC-MS based non-targeted metabolite profiling of the Chinese mitten crab *Eriocheir sinensis* suffering from hepatopancreatic necrosis disease (HPND). Aquaculture 491, 338–345.

Ginjupalli, G.K., Gerard, P.D., Baldwin, W.S., 2015. Arachidonic acid enhances reproduction in *Daphnia magna* and mitigates changes in sex ratios induced by pyriproxyfen. Environ. Toxicol. Chem. 34 (3), 527–535.

Glencross, B.D., 2009. Exploring the nutritional demand for essential fatty acids by aquaculture species. Rev. Aquac. 1, 71–124.

Gong, J., Ye, H., Xie, Y., Yang, Y., Huang, H., Li, S., Zeng, C., 2015. Ecdysone receptor in the mud crab *Scylla paramamosain*: a possible role in promoting ovarian development. J. Endocrinol. 224 (3), 273–287.

Han, T., Yang, M., Li, X., Zheng, P., Wang, C., Wang, J., 2018. Effect of dietary lipid levels on growth performance, fatty acid profile and enzymatic activity of juvenile swimming crab, *Portunus trituberculatus*. Aquac. Res. 49 (8), 2664–2670.

He, J., Wu, X.G., Li, J.Y., Huang, Q., Huang, Z.F., Cheng, Y.X., 2014. Comparison of culture and economic performance of wild-caught and pond-reared Chinese mitten crab (*Eriocheir sinensis*) juveniles reared in grow-out ponds: implications for seed selection and genetic selection programs. Aquaculture 434, 48–56.

Helland, S., Nejstgaard, J.C., Fyhn, H.J., Egge, J.K., Bamstedt, U., 2003. Effects of starvation, season, and diet on the free amino acid and protein content of *Calanus finmarchicus* females. Mar. Biol. 143, 297–306.

Holme, M.H., Southgate, P.C., Zeng, C., 2007. Survival, development and growth response of mud crab, *Scylla serrata*, megalopae fed semi-purified diets containing various fish oil: corn oil ratios. Aquaculture 269 (1–4), 427–435.

Huang, X., Feng, Y., Duan, J., Xiong, G., Fan, W., Liu, S., Yang, S., 2020. Antistarvation strategies of *E. Sinensis*: regulatory networks under hepatopancreas consumption. Oxidative Med. Cell. Longev. e6085343.

Jiang, H., Yin, Y., Zhang, X., Hu, S., Wang, Q., 2009. Chasing relationships between nutrition and reproduction: a comparative transcriptome analysis of hepatopancreas and testis from *Eriocheir sinensis*. Comp. Biochem. Phys. D 4, 227–234.

Jiang, X., Wang, H., Cheng, Y., Wu, X., 2020. Growth performance, gonad development and nutritional composition of Chinese mitten crab *Eriocheir sinensis* selected for growth and different maturity time. Aquaculture 523, 735194.

Johnston, D.J., Ritar, A.J., Thomas, C.W., 2004. Digestive enzyme profiles reveal digestive capacity and potential energy sources in fed and starved spiny lobster (*Jasus edwardsii*) phyllosoma larvae. Comp. Biochem. Physiol. 138B, 137–144.

Khatun, M.M., Kamal, D., Ikejima, K., Yi, Y., 2009. Comparisons of growth and economic performance among monosex and mixed-sex culture of red mud crab (*Scylla olivacea*

Herbst, 1796) in bamboo pens in the tidal flats of mangrove forests, Bangladesh. Aquac. Res. 40, 473–485.

Kudikina, N.P., 2011. Effect of hormonal compounds on embryogenesis of the pond snail *Lymnaea stagnalis* (L., 1758). Russ. J. Dev. Biol. 42, 180–185.

Kumar, V., Sinha, A.K., Romano, N., Allen, K.M., Bowman, B.A., Thompson, K.R., Tidwell, J.H., 2018. Metabolism and nutritive role of cholesterol in the growth, gonadal development, and reproduction of crustaceans. Rev. Fish. Sci. Aquac. 26 (2), 254–273.

Lam, S.M., Zhou, T., Li, J., Zhang, S., Chua, G.H., Li, B., Shui, G., 2020. A robust, integrated platform for comprehensive analyses of acyl-coenzyme as and acyl-carnitines revealed chain length-dependent disparity in fatty acyl metabolic fates across Drosophila development. Sci. Bull. 65 (21), 1840–1848.

Li, S., Alfaro, A.C., Nguyen, T.V., Young, T., Lulijwa, R., 2020. An integrated omics approach to investigate summer mortality of New Zealand Greenshell™ mussels. Metabolomics 16, 100.

Li, W.F., Li, S., Liu, J., Wang, X.F., Chen, H.Y., Hao, H., Wang, K.J., 2021. Vital carbohydrate and lipid metabolites in serum involved in energy metabolism during pubertal molt of mud crab (*Scylla paramamosain*). Metabolites 11, 651.

Liu, L., Fu, Y., Xiao, L., Liu, X., Fang, W., Wang, C., 2021. iTRAQ-based quantitative proteomic analysis of the hepatopancreas in *Scylla paramamosain* during the molting cycle. Comp. Biochem. Phys. D 40, 100870.

Muhd-Farouk, H., Jasmani, S., Ikhwanuddin, M., 2016. Effect of vertebrate steroid hormones on the ovarian maturation stages of orange mud crab, *Scylla olivacea* (Herbst, 1796). Aquaculture 451, 78–86.

Neiland, K.A., Scheer, B.T., 1953. The influence of fasting and of sinus gland removal on body composition of *Hemigrapsus nudus*. Physiol. Comp. Oecol. 3, 321.

Neves, C.A., Pastor, M.P., Nery, L.E., Santos, E.A., 2004. Effects of the parasite *Probopyrus ringueleti* (Isopoda) on glucose, glycogen and lipid concentration in starved *Palaemonetes argentinus* (Decapoda). Dis. Aquat. Org. 2–3, 209–213.

Nguyen, N.T.B., Chim, L., Lemaire, P., Wantiez, L., 2014. Feed intake, molt frequency, tissue growth, feed efficiency and energy budget during a molt cycle of mud crab juveniles, *Scylla serrata* (Forskål, 1775), fed on different practical diets with graded levels of soy protein concentrate as main source of protein. Aquaculture 434, 499–509.

Niu, J., Lin, H.Z., Jiang, S.G., Chen, X., Wu, K.C., Tian, L.X., Liu, Y.J., 2012. Effect of seven carbohydrate sources on juvenile *Penaeus monodon*. Anim. Feed Sci. Technol. 174, 86–95.

Oliphant, A., Alexander, J.L., Swain, M.T., Webster, S.G., Wilcockson, D.C., 2018. Transcriptomic analysis of crustacean neuropeptide signaling during the moult cycle in the green shore crab, *Carcinus maenas*. BMC Genomics 19, 711.

Phlippen, M.K., Webster, S.G., Chung, J.S., Dircksen, H., 2000. Ecdysis of decapod crustaceans is associated with a dramatic release of crustacean cardioactive peptide into the haemolymph. J. Exp. Biol. 203 (3), 521–536.

Ritar, A.J., Dunstan, G.A., Crear, B.J., Brown, M.R., 2003. Biochemical composition during growth and starvation of early larval stages of cultured spiny lobster (*Jasus edwardsii*) phyllosoma. Comp. Biochem. Physiol. 136, 353–370.

Rivera-Pérez, C., García-Carreño, F., 2011. Effect of fasting on digestive gland lipase transcripts expression in *Penaeus vannamei*. Mar. Genomics 4, 273–278.

Sánchez-Paz, A., García-Carreño, F., Muhlia-Almazán, A., Peregrino-Uriarte, A.B., Hernández-López, J., Yepiz-Plascencia, G., 2006. Usage of energy reserves in crustaceans during starvation: status and future directions. Insect Biochem. Molec. 36 (4), 241–249.

Sánchez-Paz, A., García-Carreño, F., Hernández-López, J., Muhlia-Almazán, A., Yepiz-Plascencia, G., 2007. Effect of short-term starvation on hepatopancreas and plasma energy reserves of the Pacific white shrimp (*Litopenaeus vannamei*). J. Exp. Mar. Biol. Ecol. 340, 184–193.

Shi, X., Waiho, K., Li, X., Ikhwanuddin, M., Miao, G., Lin, F., Ma, H., 2018. Female-specific SNP markers provide insights into a WZ/ZZ sex determination system for mud crabs *Scylla paramamosain*, *S. tranquebarica* and *S. serrata* with a rapid method for genetic sex identification. BMC Genomics 19, 981.

Sugumar, V., Vijayalakshmi, G., Saranya, K., 2013. Molt cycle related changes and effect of short-term starvation on the biochemical constituents of the blue swimmer crab *Portunus pelagicus*. Saudi J. Biol. Sci. 20, 93–103.

Suprayudi, M.A., Takeuchi, T., Hamasaki, K., 2004. Essential fatty acids for larval mud crab *Scylla serrata*: implications of lack of the ability to bioconvert C18 unsaturated fatty acids to highly unsaturated fatty acids. Aquaculture 231, 403–416.

Taipale, S.J., Kainz, M.J., Brett, M.T., 2011. Diet-switching experiments show rapid accumulation and preferential retention of highly unsaturated fatty acids in *Daphnia*. Oikos 120, 1674–1682.

Teshima, S., Kanazawa, A., Okamoto, H., 1977. Effects of dietary cholesterol levels on the growth, molt performance, and immunity of juvenile swimming crab, *Portunus trituberculatus*. Mar. Biol. 39, 129–136.

Wang, J., Jiang, K.J., Zhang, F.Y., Song, W., Zhao, M., Wei, H.Q., Ma, L.B., 2015. Characterization and expression analysis of the prophenoloxidase activating factor from the mud crab *Scylla paramamosain*. Genet. Mol. Res. 14 (3), 8847–8860.

Wang, W., Wu, X., Liu, Z., Zheng, H., Cheng, Y., 2014. Insights into hepatopancreatic functions for nutrition metabolism and ovarian development in the crab *Portunus trituberculatus*: gene discovery in the comparative transcriptome of different hepatopancreas stages. PLoS One 9 (1), e84921.

Wang, X., Li, E., Chen, L., 2016. A review of carbohydrate nutrition and metabolism in crustaceans. N. Am. J. Aquac. 78 (2), 178–187.

Wen, X.B., Chen, L.Q., Ai, C.X., Zhou, Z., Jiang, H., 2001. Variation in lipid composition of Chinese mitten-handed crab, *Eriocheir sinensis* during ovarian maturation. Comp. Biochem. Physiol. B 130 (1), 95–104.

Williams, G., Wood, J., Dalliston, B., Shelley, C., Kuo, C., 1999. Mud crab, *Scylla serrata* megalopa larvae exhibit high survival rates on Artemia-based diets. In: Kenaan, C.,

Blackshaw, A. (Eds.), Mud Crab Aquaculture and Biology. ACIAR, Canberra, Australia, pp. 131–137.

Yang, F., Xu, H.T., Dai, Z.M., Yang, W.J., 2005. Molecular characterization and expression analysis of vitellogenin in the marine crab *Portunus trituberculatus*. Comp. Biochem. Physiol. B 12 (4), 456–464.

Yao, G.G., Wu, X.G., Cheng, Y.X., Yang, X.Z., Wang, C.L., 2008. The changes of histology and main biochemical composition in the hepatopancreas at the different physiological stages of *Portunus trituberculatus* in East China Sea. Acta Oceanol. Sin. 30 (6), 122–131.

Yao, H., Li, X., Tang, L., Wang, H., Wang, C., Mu, C., Ce Shi, C., 2020. Metabolic mechanism of the mud crab (*Scylla paramamosain*) adapting to salinity sudden drop based on GC-MS technology. Aquacult. Rep. 18, 100533.

Zhan, Q., Han, T., Li, X., Wang, J., Yang, Y., Yu, X., Wang, C., 2020. Effects of dietary carbohydrate levels on growth, body composition, and gene expression of key enzymes involved in hepatopancreas metabolism in mud crab *Scylla paramamosain*. Aquaculture 529, 735638.

Zhou, Q.C., Shi, B., Jiao, L.F., Jin, M., Sun, P., Ding, L.Y., Yuan, Y., 2019. Hepatopancreas and ovarian transcriptome response to different dietary soybean lecithin levels in *Portunus trituberculatus*. Comp. Biochem. Phys. D 31, 100600.